



Cavity-dumped nanosecond Cr:LiSAF laser in the 985–1030 nm region for versatile seeding of Yb-based amplifiers

Umit Demirbas^{1,2} · Franz X. Kärtner^{1,3,4} · Mikhail Pergament¹

Received: 17 November 2021 / Accepted: 20 December 2021 / Published online: 9 January 2022
© The Author(s) 2022

Abstract

We report nanosecond (ns) cavity-dumped operation of a low-cost diode-pumped Cr:LiSAF laser around 1000 nm. The system is pumped with one 1-W single-emitter multimode diode at 665 nm. A Pockell cell (PC) and thin-film-polarizer (TFP) combination placed inside the cavity chops up an adjustable portion of the intracavity power and creates a variable time-dependent output coupler. Via adjusting the length and magnitude of the electrical signal going into the PC, output pulses with pulsewidths in the 2.5–500 ns range and with peak power levels above 10 W are generated at repetition rates up to 100 kHz. The central wavelength of the pulses could be smoothly tuned in the 985–1030 nm region, and is only limited by the anti-reflection coating bandwidth of the current PC and TFP. This versatile nanosecond source with 100 nJ level energies could serve as an attractive low-cost seed source for Yb-based amplifiers, including the cryogenic Yb:YLF systems.

1 Introduction

High-energy Ytterbium-based amplifiers with pulsewidths in the femtosecond to nanosecond range are desired in many applications, such as spectral broadening and compression of high-energy pulses, pumping of optical parametric amplifiers/synthesizers and Ti:Sapphire lasers, terahertz radiation generation, and laser-wakefield acceleration [1–5]. In case of Yb:YAG, the peak of the gain is centered around 1030 nm, and the systems could easily be seeded by fiber or solid-state-based Yb oscillators [6–8]. For other Yb-amplifier systems like Yb:YVO₄ [9, 10], Yb:CaF₂ [11], Yb:KYW [12], Yb:YLF [13], and Yb:LLF [14, 15], the gain spectrum covers regions well below 1030 nm, especially for oscillators that are operated at cryogenic temperatures [16–19]. As an

example, with cryogenic Yb:YLF strong amplification of ns pulses is feasible in the 985–1020 nm range with strong gain peaks located at 992.5 nm, 995.2 nm, 999.7 nm, 1006.2 nm, 1013.2 nm, 1018 nm and 1019.2 nm [20–22]. However, it is rather challenging to produce room-temperature Yb-based seed sources at these shorter wavelengths. As an example, in the case of Yb fibers, the system becomes three-level for wavelengths below 1030 nm due to the overlapping emission and absorption bands and high inversion pumping is required to attain sufficient gain at shorter wavelength side. Furthermore, to operate at high inversion, strong pumping is required, which then creates amplified spontaneous emission (ASE) issues at the 1030 nm region [23]. One alternative is to use cryogenically cooled oscillators as seed sources, but their complexity creates an additional challenge, and it is usually desired to minimize the complexity of the seeder as much as possible to direct the main attention into the high-power amplifier.

In earlier studies with cryogenic Yb:YLF, 10 s of pJ to few nJ pulses from Ti:Sapphire oscillators around 1018 nm were used as seed sources [3, 24, 25]. Ti:Sapphire systems provide broad tunability, but at this long-wavelength region, the resulting pulse energies are in the nJ range even for systems pumped with > 10 W of pump power [26–32]. Moreover, despite recent promising progress in direct diode-pumping [33], the commercial Ti:Sapphire systems still mostly rely on pumping with other lasers, making the systems rather complex, inefficient, bulky and high-cost. As an alternative,

✉ Umit Demirbas
uemit.demirbas@cfel.de

¹ Center for Free-Electron Laser Science CFEL, Deutsches Elektronen-Synchrotron DESY, Notkestr. 85, 22607 Hamburg, Germany

² Laser Technology Laboratory, Department of Electrical and Electronics Engineering, Antalya Bilim University, Antalya, Turkey

³ Physics Department, University of Hamburg, Luruper Chaussee 149, 22761 Hamburg, Germany

⁴ The Hamburg Centre for Ultrafast Imaging, Luruper Chaussee 149, 22761 Hamburg, Germany

Yb-fiber sources were also employed as seed sources for Yb:YLF for amplification around 1018 nm [23, 34], but as mentioned earlier, this wavelength region is challenging for Yb-fiber systems as well. Amplification of pulses below 1000 nm with cryogenic Yb:YLF is demonstrated only recently [35]. In this study, Manni et al. used a cryogenic multi-pass 995 nm Yb:YLF system to amplify 1 μ s long 60 nJ pulses at 40 kHz to a pulse energy of 1 mJ (average power: 40 W) [35]. The seeder had a quite long pulsewidth, and was rather complex: a single-frequency diode laser is first amplified to 1 W level via a tapered semiconductor amplifier, and later chopped into 1 μ s long pulses via combination of acousto-optic and electro-optic modulators [35].

As an attractive alternative to Ti:Sapphire system, Cr:LiSAF gain media could be directly diode-pumped in the red spectral region, and could provide broadly tunable laser output in the 770–1110 nm range with efficiencies close to 50% [36–43]. Moreover, Cr:LiSAF crystals with low passive losses (0.15% per cm) and large figure of merit (~ 3000) can also be grown rather easily [44]. Combined with a larger fluorescence lifetime (67 μ s) and emission cross-section product, this results in ultralow lasing thresholds even below a mW in Cr:LiSAF [45]. The low crystal losses further enable construction of ultrahigh-Q-cavities, which can tune to 1 μ m region even with systems pumped with 100 mW of pump power [41]. The high-Q-cavities constructed with Cr:LiSAF could store large amounts of intracavity laser power which is of great interest for minimizing laser noise such as timing jitter noise in mode-locked operation and for increasing the efficiency of intracavity nonlinear processes such as intracavity frequency-doubling [41]. Furthermore, via cavity-dumping, the stored intracavity power in the resonator could also be exploited in scaling output pulse energies. As an example, a 0.5 W diode-pumped Cr:LiSAF laser which produce around 2 nJ of pulse energies in typical mode-locked operation (200 mW at 100 MHz), could be cavity-dumped to produce pulse energies above 100 nJ level (50 times scaling in output pulse energies at the expense of reduced repetition rate: 10–1000 kHz) [46]. Note that in this cavity-dumping approach, the energy is stored in the intracavity field rather than in the laser crystal [47], and the requirement for efficient storage is to have an ultra-low loss resonator, and one is not limited by the storage lifetime of the laser crystal. As a drawback, Cr:LiSAF suffer from Auger upconversion [48], excited-state absorption [49], temperature quenching of fluorescence lifetime [50], and have a relatively low thermal conductivity (1.8 W/Km), which makes it more susceptible to thermal effects compared to Ti:Sapphire.

In this work, we have investigated the potential of Cr:LiSAF laser as a tunable nanosecond seed source for Yb-based amplifiers, especially focusing our attention on cryogenic Yb:YLF systems. Similar to Ti:Sapphire, the 1000 nm region is at the edge of the tuning range for Cr:LiSAF (ECS

is five-fold smaller compared to the peak value); hence, typical approaches do not provide pulses with high peak power/energy at this wavelength region [41, 51] (except in low-repetition-rate flashlamp/LED pumped systems [47, 52, 53]). To circumvent this limitation, as it was explored earlier [46], we have tried cavity-dumping approach to exploit the energy storage capability of Cr:LiSAF resonators to our advantage in scaling the peak powers. In the experiments, a simple low-cost diode-pumped system pumped by a 1-W single-emitter multimode diode is investigated. The ns pulses are generated via intracavity chopping of the Cr:LiSAF laser power using a fast electro-optic modulator. We have first inspected continuous-wave (cw) lasing performance and tuning behavior in the 1000 nm region for the simple/bare Cr:LiSAF laser cavity. Later, we have explored the effect of additional losses from the extra-cavity elements, such as the Pockell cell (PC) and thin-film polarizer (TFP), in cw lasing and tuning performance, as this is the key limitation for energy storage of the cavity. In cavity-dumping experiments, we have shown that, via adjusting the PC properties carefully, one can dump out pulses with pulsewidths in the 2.5–500 ns range, and with peak power levels as high as 10 W, at repetition rates up to 100 kHz. The central wavelength of the pulses could be smoothly tuned in the 985–1030 nm region. Despite the usage of a multimode pump source, via insertion of an intracavity slit near the output coupler, single longitudinal-mode operation could also be achieved to minimize mode-beating behavior. To the best of our knowledge, this is the first report of (i) high-repetition rate nanosecond pulse generation in Cr:LiSAF laser systems, and first detailed investigation of ns pulse generation around 1000 nm. We hope that, the experimental details that are shared in this initial work could be useful in producing next generation of nanosecond Cr:LiSAF seeders with much better performance than what is demonstrated in this feasibility study.

The paper is organized as follows. Section 2 provides details on the experimental setup. In Sect. 3 (a), we present cw lasing performance with a focus on cw laser performance around the 1000 nm region. Section 3 (b) discusses the cavity-dumping performance in detail, and in Sect. 4, we provide suggestions on how to possibly improve the performance in future studies. We finalize the paper with a brief conclusion in Sect. 5.

2 Experimental setup

Figure 1 shows a schematic of the cavity-dumped Cr:LiSAF laser. The system is pumped by one single-emitter multimode diode (MMD), providing up to 1 W of power around 665 nm. The MMD had an emitter size of 1 μ m \times 150 μ m (fast \times slow axes), with diffraction-limited output in the sagittal/fast axis, and an M^2 of 10 in the tangential/slow axis.

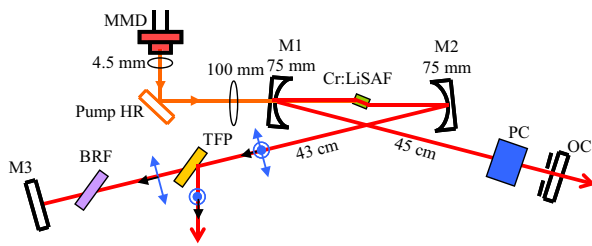


Fig. 1 A simple schematic of the diode-pumped cavity-dumped Cr:LiSAF laser. *MMD* multi-mode diode, *PC* pockell cell, *TFP* thin-film polarizer, *OC* output coupler, *BRF* birefringent filter

The MMD diode had a built-in cylindrical fiber microlens with a focal length of 100 μm , which was used to lower the divergence of the diode output in the fast axis and to minimize astigmatism at the focus. An aspherical lens with a focal length of 4.5 mm was also used to collimate the output of the MMD. The pump beam is then focused to a spot size of around $25 \mu\text{m} \times 70 \mu\text{m}$ inside the crystal using a 100 mm focal length achromatic doublet.

An astigmatically compensated, X-shaped cavity with two curved pump mirrors (M1 and M2, $R=75 \text{ mm}$), a flat end mirror (M3), and a flat output coupler (OC) was employed in the laser experiments. The pump mirrors had $> 99.98\%$ reflectivity in the 850–1120 nm wavelength range and less than 5% reflection in the 600–730 nm region. Several different output couplers (OCs) with transmission bands centered around 850 nm and 1000 nm and with output coupling changing between 0.15 and 5% were employed in analyzing the laser performance.

The cavity arms had a length of around 45 cm, resulting in a beam waist of approximately $22 \mu\text{m} \times 32 \mu\text{m}$ inside the gain medium. A vertical slit near the OC was used to control the lateral output mode of the laser in the tangential/slow axis. A 10-mm-long, 1.5% Cr-doped Cr:LiSAF crystal from VLOC was used in the study, which absorbed 99% of the incident TM polarized pump light at 665 nm. The crystal was 1.5 mm thick and mounted with indium foil in a copper holder under water cooling at 15 $^{\circ}\text{C}$. A 3-mm-thick crystal quartz birefringent filter (BRF) with an optical axis 45° to the surface of the plate was used for the tuning of the laser wavelength [54]. A thin-film polarizer (TFP) and a Pockell cell (PC) with a rise time of 8.2 ns and a fall time of 3.6 ns were used for cavity-dumping. The PC driver could be operated at up to 100 kHz, which was the limiting factor for our dumping rate. The TFP was based on fused silica, and was optimized to be used at Brewster's angle (56°) at 995 nm. One surface of the TFP was uncoated where the second surface contained a dielectric coating that is highly reflective for TE (s) polarized light ($R_s, 56^{\circ} > 99.9\%$, 900–1010 nm), and highly transmissive for the TM (p) polarized light ($R_p, 56^{\circ} < 0.5\%$, 985–1040 nm). Fine tuning of the TFP angle

enabled optimization of its wavelength working range: 5 nm shift per 1° rotation. The PC anti-reflectivity curve was optimized for a central wavelength of around 1010 nm, and its passive losses were below 1% in the 985–1045 nm region (below 0.5% in the 1005–1035 nm region). The PC at hand had two 20 mm long BBO crystals and two protective windows and was optimized to generate a $\lambda/2$ waveplate action for ring-type regenerative amplifiers [34]. Note that for the standing wave cavity as employed here, a $\lambda/4$ is sufficient for the desired cavity-dumping action. Hence, in future studies, a simpler PC with a single nonlinear crystal could be used to reduce the additional losses induced by the PC.

3 Experimental results and discussion

3.1 Continuous-wave lasing characterization

We start presenting cw lasing results with Fig. 2a, which shows the measured variation of laser output power with absorbed pump power for 1%, 3% and 5% transmitting output couplers. The datum is taken in a simple laser cavity, without the presence of intracavity elements, such as the PC, TFP and BRF. The central reflectivity bands of these three OCs were around 850 nm and hence, as indicated in figure caption, the free-running laser wavelength was close to the gain peak of Cr:LiSAF in this data. As an example, using a 1% transmitting OC, we have achieved up to 236 mW of cw laser power at 855 nm, at an absorbed pump power of 990 mW. The cw lasing threshold and the slope efficiency of the laser were 40 mW and 28%, respectively. Note that, for higher output coupling values of 3 and 5%, the lasing threshold is higher and the slope efficiency is lower. The increase in lasing threshold is due to the increasing cavity losses and the decrease in slope efficiency is due to Auger upconversion process, as discussed in earlier studies [41, 48]. Due to the difficulty in mode-matching to the multimode pump mode, the lasing threshold is rather high, and slope efficiency is rather low (30%), and both of these could be improved to 50% level via using higher brightness pump diodes [41, 51]. Moreover, due to non-optimum mode-matching, we also see onset of thermal effects even at 1 W of absorbed pump power level. The chromium doping of the Cr:LiSAF crystal could be reduced to improve thermal behavior in future studies.

Figure 2b shows the measured laser performance of the cw Cr:LiSAF laser using output couplers with reflectivity band centered around 1000 nm. For lasing around 1000 nm, the best cw performance is obtained with a 0.5% transmitting output coupler, where we have measured a cw power of 110 mW at 950 nm at an absorbed pump power of 850 mW. The cw lasing threshold and slope efficiency were measured as 43 mW and 15%, respectively. Compared to 850 nm

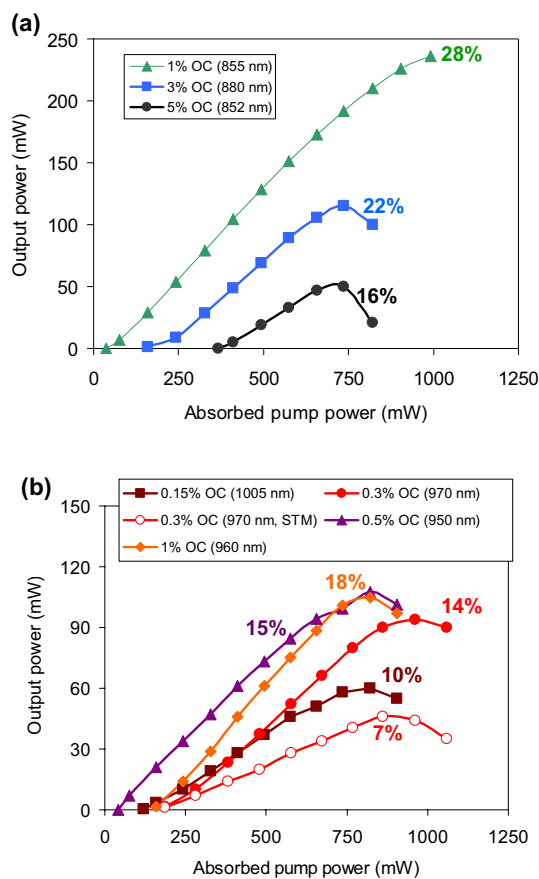


Fig. 2 Measured cw efficiency curves for the Cr:LiSAF laser, while the system is lasing around **a** 850 nm and **b** 1000 nm, respectively. The free-running cw wavelength is determined by the reflectivity range of the output couplers and it is indicated in the figure legend for each OC. Laser slope efficiency with respect to absorbed pump power is also shown for each case. For the 0.3% transmitting output coupler, STM (single-transverse mode) operation data are also presented. For other cases, the laser output is multi-transverse mode

lasing, while lasing around 1000 nm, the lasing threshold increases due to lower emission cross-sectional value, and the slope efficiency decreases due to the higher quantum defect. As expected, the thermal effects also start earlier compared to 850 nm lasing, again owing to the larger quantum defect. As a final note, the laser output was multimode (multi-transverse mode), as it is usually the case in multimode diode-pumped Cr:LiSAF lasers [41]. As shown in Fig. 2b, for the 0.3% output coupler, via adjusting the width of the intracavity vertical slit near the output coupler, it was possible to achieve single-transverse-mode (STM) operation, but this comes at the expense of reduced efficiency.

Measured cw tuning range of the Cr:LiSAF laser using several of the OCs discussed above is shown in Fig. 3a. The data were taken at an absorbed pump power of around 750 mW, and the total tuning range obtained covers the 800–1100 nm region. With the insertion of BRF, the spectral

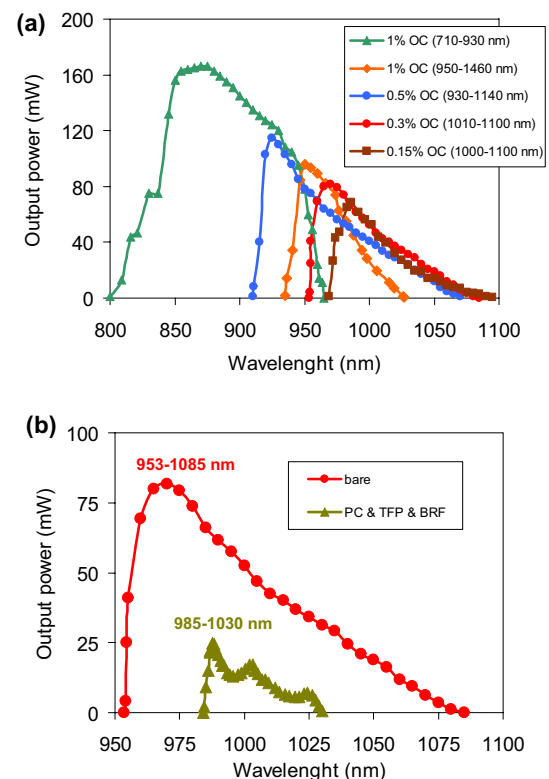


Fig. 3 a CW tuning curves of the multimode diode-pumped Cr:LiSAF laser taken using five different OCs with different coupling and reflectivity ranges. Laser wavelength could be tuned smoothly between 800 and 1100 nm using an intracavity birefringent filter. The data were taken at an absorbed pump power of 730 mW. **b** Measured cw laser tuning of the Cr:LiSAF around 1000 nm using the 0.3% output coupler for the simple and cavity-dumped cases. The tuning range and the output power levels of the cavity-dumped Cr:LiSAF laser are limited by the losses of the PC and TFP

width of the Cr:LiSAF laser decreased from 0.25–0.5 nm to sub-0.05 nm (instrument limited measurement). For each output coupler, the reflectivity bandwidth of the coating is also specified in the figure. As an example, using the 1% OC with a working range of 950–1460 nm, we have achieved lasing in the 935–1027 nm region, where the maximum cw power obtained was 96 mW at 950 nm. Note that, due to the decreased gain, for efficient lasing around 1000 nm, optimum output coupling is reduced from around 1 to 0.3%. Efficient lasing could be obtained even with a 0.15% transmitting OC, which shows that the cavity losses are rather low. As an example, with this output coupler, we have obtained up to 68 mW of cw output power at 986 nm. The intracavity stored power levels is then around 90 W level despite the usage of only 0.75 W of pump power. This intracavity power scaling capability of Cr:LiSAF makes it an ideal candidate for cavity-dumping. As a comparison, reaching this wavelength region requires 5-W of pump power in Ti:Sapphire, even using rarely found crystals with a FOM of a 1000 [32].

Basically, typical Cr:LiSAF crystals could possess FOM values in the 2000–4000 range, and could achieve long-wavelength tuning at much lower pump power levels, which significantly reduces system complexity and cost. Figure 3b shows the cw tuning curve that is achieved using the 0.3% transmitting OC after inserting the required intracavity elements for cavity-dumping (PC and TFP). The bandwidth limitations of the PC and TFP, reduced the tuning range to 985–1030 nm region. Moreover, the achievable power levels also decreased significantly due to passive losses of the PC and TFP.

To look at from another perspective, Fig. 4a displays the measured cw efficiency of the laser using the 0.3% output coupler for the bare cavity as well as for the cavity-dumped system (with additional intracavity elements). As one can see, the insertion losses of the elements required for dumping reduces the achievable output power levels from around 95 to 27 mW. We should underline here that, all of these intracavity elements were borrowed from a Yb:YLF regenerative amplifier system [34], and it should be possible to improve on their losses via optimization of their specifications (as an example the PC unit itself has eight passes though AR-coated surfaces: two nonlinear crystals and two protective windows, which could be reduced to 2 for a system optimized for losses).

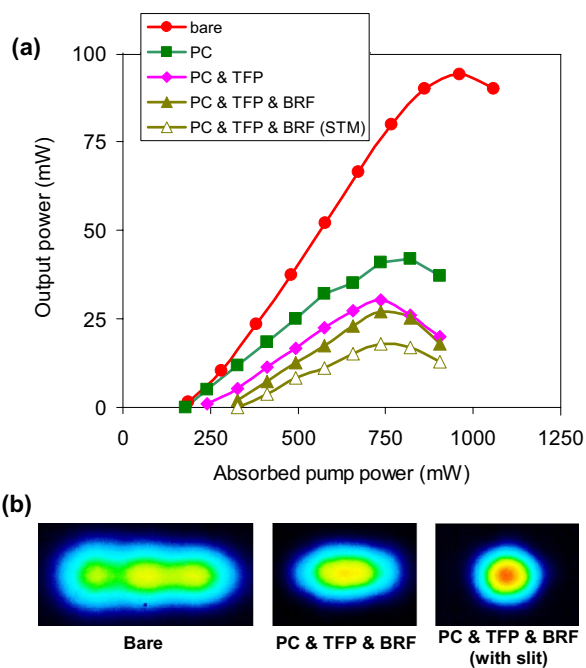


Fig. 4 **a** Measured performance of the cw Cr:LiSAF laser around 1000 nm using a 0.3% transmitting OC. The data were taken for the bare (simple) Cr:LiSAF cavity as well as for cavities with additional intracavity elements. **b** Measured output beam profile of the multi-mode diode-pumped Cr:LiSAF laser using a CCD camera at different configurations

In closing, it is elucidating to provide a little more information on the transverse-mode structure of the laser output. For that purpose, Fig. 4b shows the measured output beam profile of the laser Cr:LiSAF laser for different cases. As discussed earlier, due to the multimode diode-pumping, the Cr:LiSAF laser output is also multimode for the bare/simple Cr:LiSAF cavity. With the insertion of cavity-dumping elements, the output beam profile gets better, as the additional loss for higher-order transverse modes are larger compared to the TEM₀₀ mode. Again, using the adjustable width vertical slit near the OC mirror, single-transverse-mode operation could be achieved at the expense of reduced output power level. Note that, even for this case, the laser produced 18 mW of output power, and the intracavity laser powers are as high as 12 W. Moreover, by removing the 0.3% output coupler, the intracavity powers could easily be scaled up to 25 W level.

3.2 Cavity dumping results

We start presentation of our nanosecond cavity-dumping results with Fig. 5, which illustrates the time dynamics of the Cr:LiSAF laser intracavity power and cavity-dumped output. The data were taken while using the 0.3% transmitting OC, at a dumping rate of 100 kHz, while continuously pumping the laser with 750 mW of pump power. Figure 5a shows the typical cw operation without any dumping, and Fig. 5f shows the case with almost 100% dumping. Figures 5b–d are then the intermediate cases, which show the dynamics at different dumping ratios. While dumping at 100 kHz, the period of the dumping event is just 10 μ s, and this is faster than the lifetime of Cr:LiSAF (\sim 50 μ s under these elevated temperatures). The system does not really have time to fully recover between the dumping events, and the overshoot after the dumping could actually be used as a benefit to dump out higher energies at this repetition rate. As we see, the system is relatively stable even at dumping ratios of 80%. As long as a little portion of the intracavity power is left, as in a regenerative amplifier, the Cr:LiSAF laser uses it as a seed to amplify the circulating intracavity powers back to a similar level. Once the dumping ratio goes above 80%, as in the case of Fig. 5e, f, the system starts to be chaotic, as in a regenerative amplifier that works with too little seed power: the lasing/amplification starts back from noise like power levels, which might result in a different pulse energy at every shot. The optimum dumping rate is of course dependent on pump power level, cavity losses, and dumping rate. In general, we have seen that stable operation of the Cr:LiSAF laser is feasible at intracavity power dumping ratios up to 80–90% (higher dumping ratios could be used at lower dumping frequencies).

As a sample case, Fig. 6a shows the measured output pulse train of the cavity-dumped Cr:LiSAF laser at around

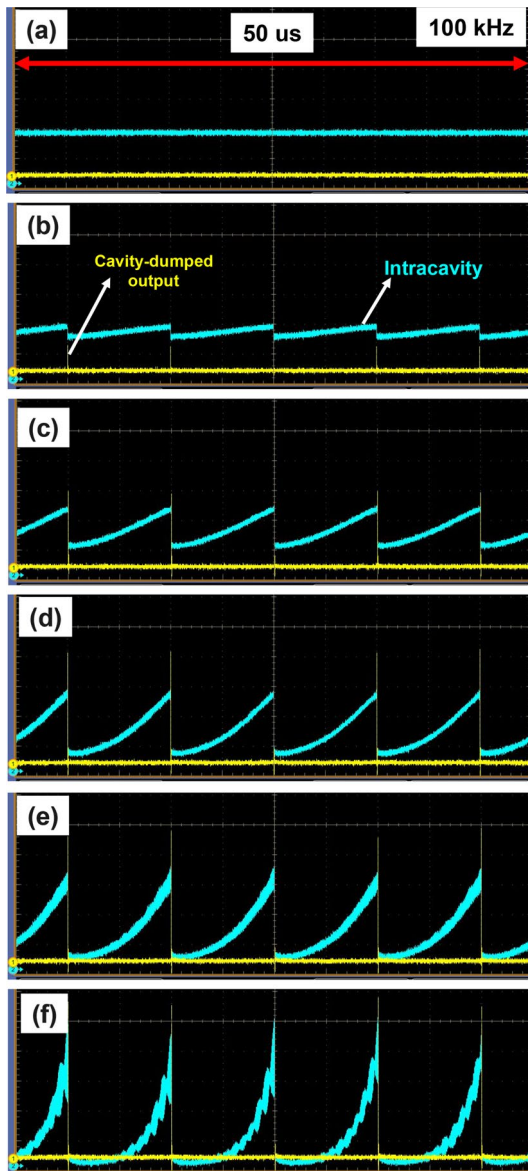


Fig. 5 Measured time dynamics of the intracavity laser (light blue) and the cavity-dumped output pulse (yellow) for the Cr:LiSAF at a dumping rate of 100 kHz. In (a–f) the cavity-dumping ratio of the intracavity power is changed slowly from 0 to 100%. For stable operation, optimum dumping ratio was around 80%, and dumping ratios above this created instability as in shown in (f). The data were taken at an absorbed pump power of 730 mW using a 0.3% OC at a lasing wavelength around 1000 nm

80% dumping ratio, for sub-15-ns long pulses with 5.85 mW average power at 100 kHz repetition rate. The shot-to-shot energy fluctuation of the output pulses was measured to be around 3%. Dumping all the intracavity power out, we could increase the output pulse energies from 58.5 nJ level to 77 nJ, but the shot-to-shot energy variation of the pulses increased to 10.3%. We have also measured the average power stability of the Cr:LiSAF laser output in cw regime,

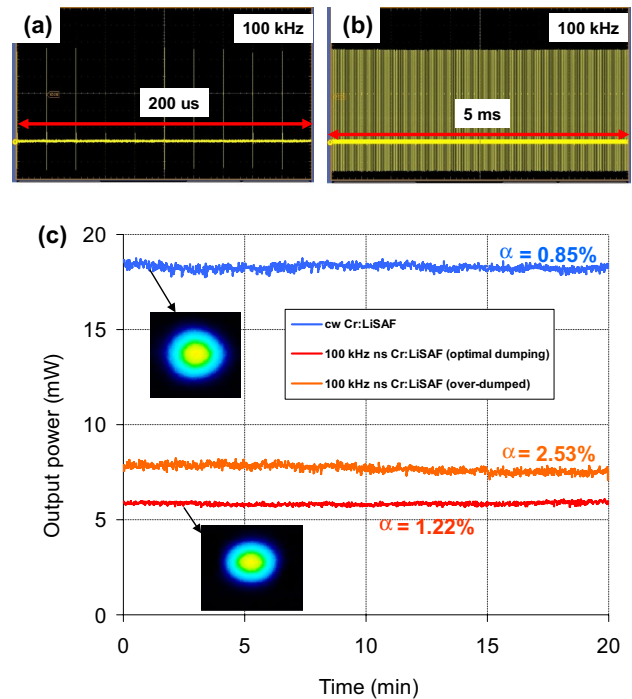


Fig. 6 Measured time dynamics of the cavity-dumped Cr:LiSAF laser output at 100 kHz dumping rate in different time scales: **a** 200 μ s, **b** 2 ms. **c** Measured variation of cw Cr:LiSAF laser output power, and cavity-dumped Cr:LiSAF laser average power at 100 kHz dumping rate. The average power of the cavity-dumped laser is taken at cavity-dumping ratios of around 80% and 100%, to show the resulting increase of power fluctuations for the over-dumped case. The data were taken at an absorbed pump power of 730 mW using a 0.3% output coupler at a lasing wavelength around 1000 nm. The inset figures show the measured beam profiles of the laser output

as well as in cavity-dumped cases. For the cavity-dumped case, power stability is investigated in \sim 80% and \sim 100% dumped cases. The data are taken for a 20 min interval and is shown in Fig. 6b. As we see, the Cr:LiSAF laser itself has a power fluctuation of 0.85% rms (ratio of standard deviation in output power to mean output power value). For the 80% dumped case, the power fluctuations of the Cr:LiSAF laser are around 1.22%, which increases to 2.53% for the fully dumped case.

We have observed a similar behavior in the radio frequency (RF) spectrum data we have taken. Figure 7a, b, shows the cases where the dumping rate is kept around 80%, and Fig. 7c illustrates the case for a fully dumped Cr:LiSAF oscillator. As we see in Fig. 7a, b, for optimized dumping rate, a clean RF spectrum with peaks at multiples of 100 kHz is visible, and the main peaks are around 60 dBm above the noise level. On the other hand, for the over-dumped case, the background noise level increases 10–20 dBm, and additional sub-peaks also appear at 35.5 kHz, 64.5 kHz (100–35.5 kHz), 135.5 kHz (100+35.5 kHz): showing that the Cr:LiSAF laser dynamics creates some oscillations

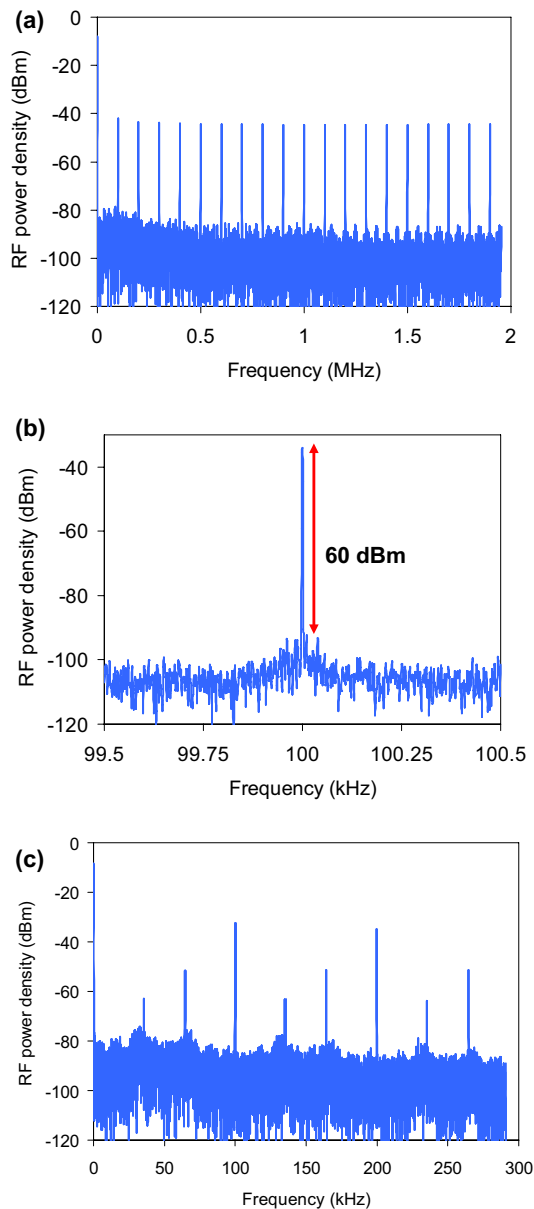


Fig. 7 Radio frequency (RF) spectrum of the cavity-dumped Cr:LiSAF laser at a dumping ratio of (a, b) 80% and (c) 95–100%, for a dumping rate of 100 kHz. The RF spectrum shows stable pulsing in (a, b) for reasonably dumped cavity, whereas over-dumping of the laser created large fluctuations as shown in (c). **a** RF centered at 1 MHz with a span of 2 MHz, and resolution bandwidth of 100 Hz, **b** RF centered at 100 kHz with a span of 1 kHz and resolution bandwidth of 1 Hz, **c** RF centered at 150 kHz with a span of around 300 kHz and resolution bandwidth of 20 Hz. The data were taken at an absorbed pump power of 730 mW using a 0.3% OC at a lasing wavelength around 1000 nm

at around 35.5 kHz in this configuration (as it is also visible in Fig. 5f). As a side note, while taking these data, the Cr:LiSAF laser was not covered, and it was open to air fluctuations. Hence, future reduction of noise should be feasible in well-engineered cavities.

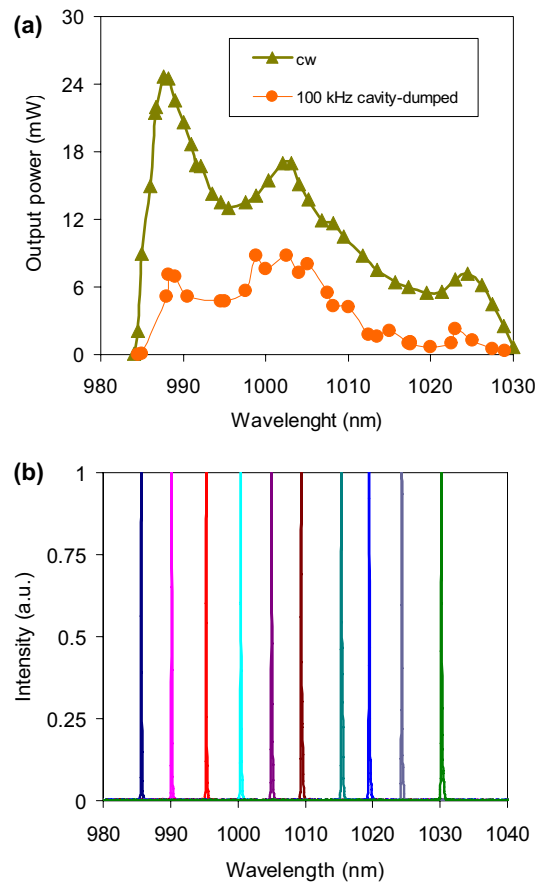


Fig. 8 **a** Measured variation of the cavity-dumped Cr:LiSAF laser average output power with wavelength. The cw tuning curve with a 0.3% OC is also shown for comparison. **b** Sample optical spectra of the cavity-dumped Cr:LiSAF laser. The data were taken at an absorbed pump power of 730 mW, and at a dumping rate of 100 kHz

Note that it was possible to tune the central wavelength of the pulses rather smoothly via rotation of the intracavity birefringent filter. Figure 8a shows the measured variation of cavity-dumped Cr:LiSAF laser average output power as a function of central wavelength of the pulses for the dumping rate of 100 kHz. Sample optical spectra at different wavelengths are shown in Fig. 8b. As discussed in the experimental part, the PC and the TFP used in this study had coatings that is optimized for 995–1015 nm operation and was borrowed from a Yb:YLF regenerative amplifier system [34]. As a result, especially the narrow coating bandwidth of the TFP limited the tuning range to 985–1030 nm region. Figure 8a also shows the measured cw tuning with the 0.3% output coupler (while the PC is off). The fluctuations observed in laser power (e.g., the dip around 995 nm) are similar in both cw tuning and cavity-dumping curves. This shows that these power fluctuations are due to the reflectivity oscillations of the TFP and PC coatings, and is not a result of PC operation. Ideally, using an acousto-optic dumper, one

can improve the tuning bandwidth of the nanosecond pulses considerably.

Besides looking at the effect of dumping ratio, we have also tested the effect of PC pulsewidth on cavity-dumped Cr:LiSAF laser output parameters. Here, by PC pulsewidth, we mean the electrical signal width that we send to the PC driver, and of course due to the limited response time of the driver electronics, the actual pulsewidth of the retardation that the PC generates could be longer for very short electrical pulses. In an extra-cavity setup, we have tested the PC and we have seen that, the PC could generate $\lambda/4$ waveplate action for pulses with a minimum full-width at half maximum (FWHM) of around 10 ns. This agrees with the specifications of the PC driver (rise time: 8.2 ns, fall time:

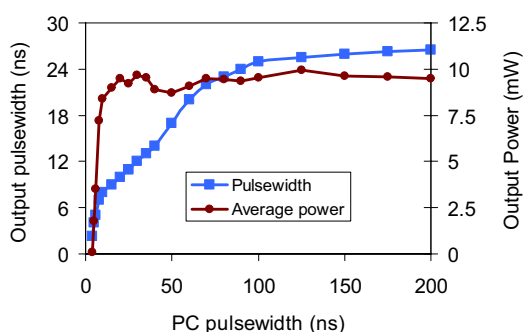
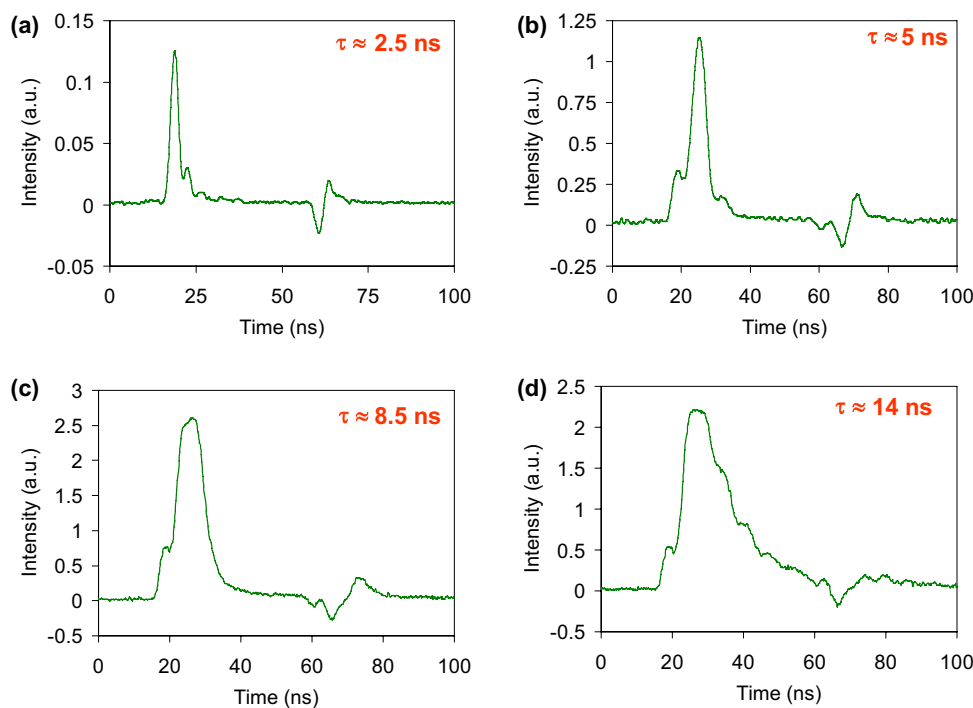


Fig. 9 Measured variation of laser output pulsewidth and average output power as a function of the PC electrical gate signal width. The data were taken at a dumping rate of 100 kHz and at an absorbed pump power of 730 mW using a 0.3% transmitting OC

3.6 ns, estimated minimum response time: 11.8 ns). On the other hand, pulses even shorter than 5 ns were also feasible, but at the expense of reduced waveplate action (reaching $\lambda/4$ was not possible).

Figure 9a shows the measured variation of cavity-dumped Cr:LiSAF laser average output power and pulsewidth as a function of the length of the PC electrical signal. One can see that, the PC could provide enough waveplate action for pulsewidths above 10 ns, as it could successfully dump out at least 70–80% of the intracavity laser power and could generate around 9 mW average output power. On the other hand, for PC electrical signals that are shorter than 10 ns, the average power of the cavity-dumping decreased in a sharp manner. In terms of obtainable output pulsewidths, we could generate pulsewidths as short as 2.5 ns, but only at an average power of around 0.075 mW (0.75 nJ energy), due to the decreasing waveplate action of the PC (or lower dumping ratio of the PC). When we focus on the efficient working range of the PC (10–200 ns driving signal pulsewidth range), we see that the pulsewidth of the cavity-dumped Cr:LiSAF laser could be easily adjusted between 8 and 25 ns. Figure 10 shows sample pulsewidth measurements for the cavity-dumped Cr:LiSAF laser for output pulsewidths of (a) 2.5 ns, (b) 5 ns, (c) 8.5 ns, and (d) 14 ns. Note that, the output pulsewidth of the cavity-dumped laser depends on many factors: (i) the pulsewidth applied to the DG as already discussed, (ii) the modulation depth of the dumping (dumping ratio), (iii) and Cr:LiSAF laser cavity dynamics. The data in Figs. 9 and 10 are taken while optimizing the

Fig. 10 Fast photodiode traces of the cavity-dumped Cr:LiSAF laser in short-pulse configuration for sample pulsewidths of **a** 2.5 ns, **b** 5 ns, **c** 8.5 ns and **d** 14 ns. The data were taken at a dumping rate of 100 kHz and at an absorbed pump power of 730 mW using a 0.3% OC. The oscillation following the main pulse is due to the ringing of the photodetector



dumping ratio for each case to get the highest output energy: lower dumping ratio is applied for longer pulses.

As we see from the data in Fig. 9, even for a 200 ns PC electrical signal, the obtained output pulse length was around 25 ns. This is because the data in Fig. 9 are taken at optimum output pulse energy conditions. To elaborate on this issue further, Fig. 11 shows the effect of dumping ratio on the obtainable pulsewidths for two samples: (a) for a 50 ns long PC dumping signal, and in (b) for a 500 ns long PC dumping signal. As we see, for longer PC timing signals, when one aims to optimize the dumped output energy, this requires a larger dumping ratio. Then, since the intracavity circulating power is reduced significantly, the cavity-dumped Cr:LiSAF peak power also decays in a fast manner, creating pulses with a FWHM shorter than the pulsewidth employed to the PC. On the other hand, if one lowers the dumping ratio to a level that does not significantly alter the intracavity power levels, the output pulse length increases and could have a length similar to the length of PC signal. However, of course, the peak power of the dumped pulses is

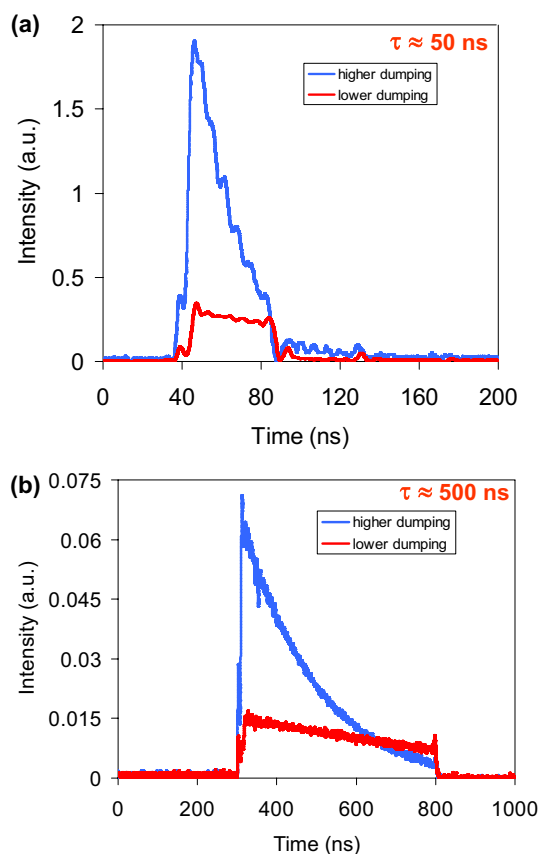


Fig. 11 Fast photodiode traces of the cavity-dumped Cr:LiSAF laser in long-pulse configuration for sample pulsewidths of **a** 50 ns, **b** 500 ns. The measured time profile is shown for different cavity-dumping ratios. The data were taken at a dumping rate of 100 kHz and at an absorbed pump power of 730 mW using a 0.3% transmitting OC

lower in this case and the average power and pulse energy also somehow decay. In short, via adjusting the PC timing, we could tune the output pulsewidth of the cavity-dumped Cr:LiSAF laser in the 2.5–500 ns range (longer pulsewidths are also feasible). However, the system was operating more efficiently for output pulsewidths in the 8–25 ns range: (i) for pulses in the 2.5–8 ns interval, the limited PC driver timing response reduces the obtainable pulse energies, and (ii) for pulsewidths longer than 25 ns, the Cr:LiSAF laser dynamics limited the performance.

Another test we have performed was to check the variation of output pulse energy as a function of repetition rate. Figure 12 shows this behavior for dumping frequencies between 1 Hz and 100 kHz. The output energies at higher repetition rates are calculated using the measured average power of the pulse train. We have also used a fast Si detector and an oscilloscope and calibrated the measured response of the system at 100 kHz with the average power measurements. The calibrated curve is then used to estimate the pulse energy at lower repetition rates. The good match of energies estimated via the power meter and the calibrated Si detector in the 20–100 kHz range confirms the usability of the Si detector in estimating energies for lower rep rates. As we see from Fig. 12, for repetition rates between 1 Hz and 5 kHz, the output pulse energy did not change much and stayed around 60 nJ level. This is expected of course, since for the 5 kHz dumping rate, the period of the pulses is 200 μ s, and this is around 4 times longer than the Cr:LiSAF lifetime: hence for repetition rate of 5 kHz and below the cavity has enough time to stabilize back. We clearly see this behavior in Fig. 13, which shows the timing dynamics of the cavity-dumped Cr:LiSAF laser at dumping rates between 100 Hz and 50 kHz. As mentioned earlier, for dumping rates above 5 kHz, at some specific dumping frequencies, the dumping event could happen while the Cr:LiSAF laser is overshooting, which can be used to obtain higher pulse

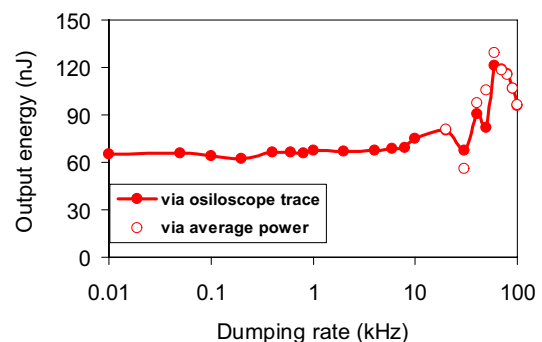


Fig. 12 Variation of the cavity-dumped Cr:LiSAF laser output energy as a function of dumping rate. The data were taken at an absorbed pump power of 730 mW using a 0.3% transmitting output coupler, while using a PC on signal with a length of 15 ns



Fig. 13 Measured time dynamics of intracavity laser power and output pulse for the cavity-dumped Cr:LiSAF at different dumping rates between 100 Hz and 50 kHz. The data were taken at an absorbed pump power of 730 mW using a 0.3% transmitting OC, while using a PC on signal with a length of 15 ns

energies. As an example, we could able to dump out pulse energies up to 130 nJ at a repetition rate of 60 kHz (a twofold improvement compared to the standard 60 nJ we get at other repetition rates).

As a final note, we want to finish the discussion with Fig. 14, which shows the intracavity dynamics of the Cr:LiSAF laser while the laser was operating in multi-mode regime (multi-transverse mode, without the intracavity slit in the cavity). Here, one can easily see the mode-beating in the intracavity circulating laser power as well as in the cavity-dumped laser output. The beating shown in Fig. 14 was due to beating of the transverse modes, but we have also

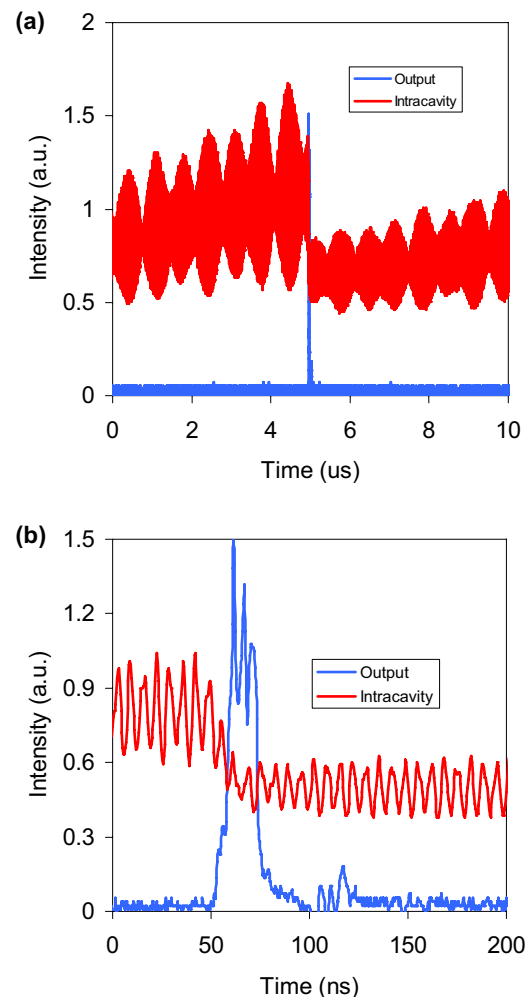


Fig. 14 Typical mode-beating behavior in the Cr:LiSAF laser causing intensity fluctuations. The mode-beating in this case was due to interference of the transverse modes, which we could prevent via pushing the laser to operate in TEM₀₀ mode using the intracavity slit. A similar behavior could also be observed in case of beating of longitudinal laser modes, which could be avoided by single-frequency operation

observed beating due to interference of longitudinal laser modes. Via putting the intracavity slit, we could remove the beating due to transverse modes, but ideally one can use a higher brightness diode to directly achieve TEM₀₀ operation from the Cr:LiSAF laser [41]. Moreover, the beating due to the longitudinal cavity modes could also be minimized via alignment of cavity (as the data in Figs. 5 and 13 show, this could be achieved up to a point: we believe this minimization is an averaging effect due to coexistence of many longitudinal modes). We have also tried to implement a 2 mm thick etalon inside the cavity to reduce beating due to longitudinal cavity modes, which helped but did not provide a perfect solution. Hence, in future studies, by building a ring-type cavity rather than a standing wave cavity, and using

several intracavity etalons, single-frequency operation could be used to truly obtain a beating-free operation. Another alternative would be seeding of the system via a low-power single-frequency diode, and operating the Cr:LiSAF as a regenerative amplifier [55]. Both approaches will require usage of low passive loss elements to not hinder the intracavity power levels.

4 Suggestions for future work

During our experimental campaign, we have realized that the performance of the current system could potentially be improved in several ways, and some of the improvements are already discussed along the text. Here, we wanted to share them again together in a little bit more detail.

First, a single 1 W low-brightness multimode diode is used in this initial study, but the Cr:LiSAF laser system inherently needs a single longitudinal-mode operation for minimization of mode-beating, which required use of an intracavity slit to push the system into TEM₀₀ operation at the expense of reduced efficiency. Hence, in future studies, use of higher brightness single-mode diodes (210 mW is now available), or tapered diodes (1 W [56]) with better beam profile could significantly improve the output beam quality and laser efficiency. In the case of single-mode diodes, use of several diodes might be required to achieve similar energies, but the efficiency of the system will be much higher.

Moreover, we have used a PC and TFP combination and created a time-dependent output coupler based on polarization rotation. This enabled flexible adjustment of output pulsewidth, but the additional losses limited the achievable energies and the tuning range. As a first step, one can use a single-crystal Pockell cell (rather than the two crystal PC) to minimize losses. Furthermore, an acousto-optic modulator/deflector (AOM) could also be used as an output coupler [46]. As an advantage, an AOM is inserted at Brewster's angle and does not require coatings, and will have much lower passive losses. Due to lower losses, one can reach higher pulse energies, and the tuning range of the ns pulses ideally covers the whole Cr:LiSAF gain spectrum (770–1110 nm). As a disadvantage, one needs to have a tight focus on the AOM cell to get a fast timing response, and this requires additional cavity elements to create a second focus. Alignment of the AOM cell and getting high diffraction efficiencies are also more challenging, which increase the complexity of the system. Moreover, one will also lose the capability to adjust the output pulsewidths: the pulsewidth will be fixed to around 10 ns in AOM dumped cavity.

Finally, we have used a 10 mm long 1.5% Cr-doped LiSAF sample in this work, and thermal effects were already present. Ideally, a 0.75% Cr-doped 10–15 mm long sample

could still absorb enough of the pump light and enable better performance due to minimization of thermal issues. A lower Cr-doped LiSAF sample potentially has lower passive losses as well, which could improve the amount of intracavity power that could be stored in the cavity.

5 Conclusion

In conclusion, we have performed a feasibility study with Cr:LiSAF and showed tunable pulsewidth (2.5 ns to 0.5 μ s) and tunable wavelength (985–1030 nm) cavity-dumped operation at repetition rates up to 100 kHz, with pulse peak power levels up to 10 W and pulse energies up to 100 nJ. Compared to other approaches (ns chopping of a cw diode and further then amplification in a few stages), the system is simpler, it is more flexible and could provide higher-peak power. On the other hand, the proof-of-principle system demonstrated in this work is not single-frequency and beating issues might be a problem while seeding high-power amplifiers. Hence, future work is required to achieve single-frequency operation, and this might be challenging due to the requirement to use lower loss elements for frequency selection.

Acknowledgements UD acknowledges support from BAGEP Award of the Bilim Akademisi.

Funding Open Access funding enabled and organized by Projekt DEAL. Seventh Framework Programme (FP7) FP7/2007-2013 European Research Council (ERC) (609920).

Declarations

Conflict of interest The authors declare that they have no conflicts of interest.

Open Access This article is licensed under a Creative Commons Attribution 4.0 International License, which permits use, sharing, adaptation, distribution and reproduction in any medium or format, as long as you give appropriate credit to the original author(s) and the source, provide a link to the Creative Commons licence, and indicate if changes were made. The images or other third party material in this article are included in the article's Creative Commons licence, unless indicated otherwise in a credit line to the material. If material is not included in the article's Creative Commons licence and your intended use is not permitted by statutory regulation or exceeds the permitted use, you will need to obtain permission directly from the copyright holder. To view a copy of this licence, visit <http://creativecommons.org/licenses/by/4.0/>.

References

1. M. Siebold, J. Hein, C. Wandt, S. Klingebiel, F. Krausz, S. Karsch, High-energy, diode-pumped, nanosecond Yb:YAG MOPA system. *Opt. Express* **16**(6), 3674 (2008)

2. H. Fattahi, H.G. Barros, M. Gorjan, T. Nubbemeyer, B. Alsaif, C.Y. Teisset, M. Schultze, S. Prinz, M. Haefner, M. Ueffing, A. Alismail, L. Vamos, A. Schwarz, O. Pronin, J. Brons, X.T. Geng, G. Arisholm, M. Ciappina, V.S. Yakovlev, D.E. Kim, A.M. Azzeer, N. Karpowicz, D. Sutter, Z. Major, T. Metzger, F. Krausz, Third-generation femtosecond technology. *Optica* **1**(1), 45–63 (2014)
3. K. Yamakawa, M. Aoyama, Y. Akahane, K. Ogawa, K. Tsuji, A. Sugiyama, T. Harimoto, J. Kawanaka, H. Nishioka, M. Fujita, Ultra-broadband optical parametric chirped-pulse amplification using an Yb:LiYF₄ chirped-pulse amplification pump laser. *Opt. Express* **15**(8), 5018 (2007)
4. H. Cankaya, A.L. Calendron, C. Zhou, S.H. Chia, O.D. Mucke, G. Cirmi, F.X. Kartner, 40-mJ passively CEP-stable seed source for ytterbium-based high-energy optical waveform synthesizers. *Opt. Express* **24**(22), 25169–25180 (2016)
5. D.F. Zhang, A. Fallahi, M. Hemmer, X.J. Wu, M. Fakhari, Y. Hua, H. Cankaya, A.L. Calendron, L.E. Zapata, N.H. Matlis, F.X. Kartner, Segmented terahertz electron accelerator and manipulator (STEAM). *Nat. Photonics* **12**(6), 336 (2018)
6. T. Dietz, M. Jenne, D. Bauer, M. Scharun, D. Sutter, A. Killi, Ultrafast thin-disk multi-pass amplifier system providing 1.9 kW of average output power and pulse energies in the 10 mJ range at 1 ps of pulse duration for glass-cleaving applications. *Opt. Express* **28**(8), 11415–11423 (2020)
7. L.E. Zapata, H. Lin, A.L. Calendron, H. Cankaya, M. Hemmer, F. Reichert, W.R. Huang, E. Granados, K.H. Hong, F.X. Kartner, Cryogenic Yb:YAG composite-thin-disk for high energy and average power amplifiers. *Opt. Lett.* **40**(11), 2610–2613 (2015)
8. C. Baumgarten, M. Pedicone, H. Bravo, H. Wang, L. Yin, C.S. Menoni, J.J. Rocca, B.A. Reagan, 1 J, 05 kHz repetition rate picosecond laser. *Opt. Lett.* **41**(14), 3339 (2016)
9. A. Rudenkov, V. Kisel, V. Matrosov, N. Kuleshov, 200 kHz 55 W Yb³⁺: YVO₄-based chirped-pulse regenerative amplifier. *Opt. Lett.* **40**(14), 3352 (2015)
10. A.E. Troshin, F. Brunner, F. Morier-Genoud, M.I. Kupchenko, N.V. Kuleshov, R. Paschotta, T.A. Matrosova, U. Keller, V.E. Kisel, V.G. Shcherbitsky, V.N. Matrosov, Femtosecond pulse generation with a diode-pumped Yb³⁺:YVO₄ laser. *Opt. Lett.* **30**(10), 1150–1152 (2005)
11. J. Körner, V. Jambunathan, J. Hein, R. Seifert, M. Loeser, M. Siebold, U. Schramm, P. Sikocinski, A. Lucianetti, T. Mocek, M.C. Kaluza, Spectroscopic characterization of Yb³⁺-doped laser materials at cryogenic temperatures. *Appl. Phys. B Lasers Opt.* **116**(1), 75–81 (2014)
12. J. Korner, M. Kruger, J. Reiter, A. Munzer, J. Hein, M.C. Kaluza, Temperature dependent spectroscopic study of Yb³⁺-doped KG(WO₄)₂, KY(WO₄)₂, YAlO₃ and YLiF₄ for laser applications. *Opt. Mater. Express* **10**(10), 2425–2438 (2020)
13. J. Kawanaka, H. Nishioka, N. Inoue, K. Ueda, Tunable continuous-wave Yb : YLF laser operation with a diode-pumped chirped-pulse amplification system. *Appl. Opt.* **40**(21), 3542–3546 (2001)
14. F. Pirzio, S. Jun, S. Tacchini, A. Di Lieto, G. Piccinno, M. Tonelli, A. Agnesi, Multi-watt amplification in a birefringent Yb:LiLuF₄ single crystal fiber grown by micro-pulling-down. *Opt. Lett.* **44**(17), 4095 (2019)
15. S. Cante and J. I. Mackenzie, "Spectroscopic characterisation of Yb:LiLuF₄ between (63–293)K," in *Optics InfoBase Conference Papers* (OSA - The Optical Society, 2019), **Part F139-ASSL 2019**, p. JM5A.4.
16. D. Rand, D. Miller, D.J. Ripin, T.Y. Fan, Cryogenic Yb³⁺-doped materials for pulsed solid-state laser applications [Invited]. *Opt. Mater. Express* **1**(3), 434–450 (2011)
17. T.Y. Fan, D.J. Ripin, R.L. Aggarwal, J.R. Ochoa, B. Chann, M. Tilleman, J. Spitzberg, Cryogenic Yb³⁺-doped solid-state lasers. *Ieee J. Sel. Top. Quantum Electron.* **13**(3), 448–459 (2007)
18. J. Kawanaka, K. Yamakawa, H. Nishioka, K. Ueda, Improved high-field laser characteristics of a diode-pumped Yb: LiYF₄ crystal at low temperature. *Opt. Express* **10**(10), 455–460 (2002)
19. J. Kawanaka, S. Tokita, H. Nishioka, M. Fujita, K. Yamakawa, K. Ueda, Y. Izawa, Dramatically improved laser characteristics of diode-pumped Yb-doped materials at low temperature. *Laser Phys.* **15**(9), 1306–1312 (2005)
20. U. Demirbas, J. Thesinga, M. Kellert, F.X. Kärtner, M. Pergament, Detailed investigation of absorption, emission and gain in Yb:YLF in the 78–300 K range. *Opt. Mater. Express* **11**(2), 250–272 (2021)
21. G. Brasse, P. Loiko, C. Grygiel, A. Benayad, F. Lemarie, V. Zakharov, A. Veniaminov, J.L. Doualan, A. Braud, P. Camy, Liquid Phase Epitaxy growth, structure and spectroscopy of highly-doped 20 at.% Yb³⁺:LiYF₄ thin films. *J. Lumin.* **236**, 118071 (2021)
22. S. Püschel, S. Kalusniak, C. Kränkel, H. Tanaka, Temperature-dependent radiative lifetime of Yb:YLF: refined cross sections and potential for laser cooling. *Opt. Express* **29**(7), 11106 (2021)
23. Y. Hua, W. Liu, M. Hemmer, L.E. Zapata, G.J. Zhou, D.N. Schimpf, T. Eidam, J. Limpert, A. Tunnermann, F.X. Kartner, G.Q. Chang, 87-W 1018-nm Yb-fiber ultrafast seeding source for cryogenic Yb: yttrium lithium fluoride amplifier. *Opt. Lett.* **43**(8), 1686–1689 (2018)
24. J. Kawanaka, K. Yamakawa, H. Nishioka, K. Ueda, 30-mJ, diode-pumped, chirped-pulse Yb: YLF regenerative amplifier. *Opt. Lett.* **28**(21), 2121–2123 (2003)
25. D.E. Miller, L.E. Zapata, D.J. Ripin, T.Y. Fan, Sub-picosecond pulses at 100 W average power from a Yb:YLF chirped-pulse amplification system. *Opt. Lett.* **37**(13), 2700–2702 (2012)
26. C. Ruppert, M. Betz, Generation of 30 femtosecond, 900–970 nm pulses from a Ti:sapphire laser far off the gain peak. *Opt. Express* **16**(8), 5572 (2008)
27. J. Wei, X. Cao, P. Jin, J. Su, H. Lu, K. Peng, Diving angle optimization of BRP in a single-frequency continuous-wave wideband tunable titanium:sapphire laser. *Opt. Express* **29**(5), 6714 (2021)
28. C. Zimmermann, V. Vuletic, A. Hemmerich, L. Ricci, T.W. Hänsch, Design for a compact tunable Ti:sapphire laser. *Opt. Lett.* **20**(3), 297 (1995)
29. B. Jungbluth, J. Wueppen, J. Geiger, B. Bach-Zelewski, N. Pirch, D. Hoffmann, P. Loosen, and R. Poprawe, "High performance widely tunable Ti:Sapphire laser with nanosecond pulses," in *Solid State Lasers XV: Technology and Devices*, H. J. Hoffman and R. K. Shori, eds. (SPIE, 2006), **6100**, p. 61000R.
30. P. Lottigier, A. Jucha, L. Cabaret, C. Blondel, C. Drag, Single-mode scannable nanosecond Ti: sapphire laser for high-resolution two-photon absorption laser-induced fluorescence (TALIF). *Appl. Phys. B Lasers Opt.* **125**(1), 14 (2019)
31. P.F. Moulton, J.G. Cederberg, K.T. Stevens, G. Foundos, M. Koselja, J. Preclikova, Characterization of absorption bands in Ti: sapphire crystals. *Opt. Mater. Express* **9**(5), 2216 (2019)
32. J.F. Pinto, L. Esterowitz, G.H. Rosenblatt, M. Kokta, D. Peressini, Improved Ti: sapphire laser performance with new high figure of merit crystals. *Ieee J. Quantum Electron.* **30**(11), 2612–2616 (1994)
33. P.W. Roth, A.J. Maclean, D. Burns, A.J. Kemp, Directly diode-laser-pumped Ti: sapphire laser. *Opt. Lett.* **34**(21), 3334–3336 (2009)
34. U. Demirbas, M. Kellert, J. Thesinga, Y. Hua, S. Reuter, M. Pergament, F.X. Kärtner, Highly efficient cryogenic Yb:YLF regenerative amplifier with 250 W average power. *Opt. Lett.* **46**(16), 3865–3868 (2021)
35. J. Manni, D. Harris, T.Y. Fan, High-gain (43 dB), high-power (40 W), highly efficient multipass amplifier at 995 nm in Yb:LiYF₄. *Opt. Commun.* **417**, 54–56 (2018)

36. S.A. Payne, L.L. Chase, L.K. Smith, W.L. Kway, H.W. Newkirk, Laser performance of LiSAIF6:Cr³⁺. *J. Appl. Phys.* **66**(3), 1051–1056 (1989)
37. S. Uemura, K. Torizuka, Generation of 10 fs pulses from a diode-pumped Kerr-lens mode-locked Cr: LiSAF laser. *Jpn. J. Appl. Phys. Part 1-Regular Pap. Short Notes Rev. Pap.* **39**(6), 3472–3473 (2000)
38. J.M. Hopkins, G.J. Valentine, B. Agate, A.J. Kemp, U. Keller, W. Sibbett, Highly compact and efficient femtosecond Cr: LiSAF lasers. *IEEE J. Quantum Electron.* **38**(4), 360–368 (2002)
39. V.G. Savitski, N.K. Metzger, S. Calvez, D. Burns, W. Sibbett, C.T.A. Brown, Optical trapping with “on-demand” two-photon luminescence using Cr:LiSAF laser with optically addressed saturable Bragg reflector. *Opt. Express* **20**(7), 7066 (2012)
40. R.E. Samad, S.L. Baldochi, G.E. Calvonogueira, N.D. Vieira Jr., 30 W Cr:LiSrAlF₆ flashlamp-pumped pulsed laser. *Opt. Lett.* **32**(1), 50 (2007)
41. U. Demirbas, Cr:Colquiriite Lasers: Current status and challenges for further progress. *Prog. Quantum Electron.* **68**, 100227 (2019).
42. F. Canbaz, N. Kakenov, C. Kocabas, U. Demirbas, A. Sennaroglu, Generation of sub-20-fs pulses from a graphene mode-locked laser. *Opt. Express* **25**(3), 2834 (2017)
43. R. Scheps, J.F. Myers, H.B. Serreze, A. Rosenberg, R.C. Morris, M. Long, Diode-pumped Cr:LiSrAlF₆ laser. *Opt. Lett.* **16**(11), 820–822 (1991)
44. D. Klimm, G. Lacayo, P. Reiche, Growth of Cr: LiCaAlF₆ and Cr: LiSrAlF₆ by the Czochralski method. *J. Cryst. Growth* **210**(4), 683–693 (2000)
45. V. Kubecek, R. Quintero-Torres, J.C. Diels, Ultralow-pump-threshold laser diode pumped Cr: LiSAF laser. *Adv. Lasers Syst.* **5137**, 43–47 (2002)
46. U. Demirbas, K.-H. Hong, J.G. Fujimoto, A. Sennaroglu, F.X. Kärtner, Low-cost cavity-dumped femtosecond Cr:LiSAF laser producing > 100 nJ pulses. *Opt. Lett.* **35**(4), 607–609 (2010)
47. P. Pichon, H. Taleb, F. Druon, J.-P. Blanchot, P. Georges, F. Balembois, Tunable UV source based on an LED-pumped cavity-dumped Cr:LiSAF laser. *Opt. Express* **27**(16), 23446 (2019)
48. S.A. Payne, L.K. Smith, R.J. Beach, B.H.T. Chai, J.H. Taasano, L.D. DeLoach, W.L. Kway, R.W. Solarz, W.F. Krupke, Properties of Cr:LiSrAlF₆ Crystals for laser operation. *Appl. Opt.* **33**(24), 5526–5536 (1994)
49. W.R. Rapoport, M.L. Shand, Excited state absorption and upconversion in Cr:LiSrAlF₆. *Solid State Commun.* **84**(1–2), 29–31 (1992)
50. M. Stalder, M. Bass, B.H.T. Chai, Thermal quenching of fluorescence in chromium-doped fluoride laser crystals. *J. Opt. Soc. Am. B* **9**(12), 2271–2273 (1992)
51. U. Demirbas, J. Thesinga, M. Kellert, S. Reuter, B. Sumpf, M. Pergament, and F. X. Kärtner, “Mode-locked Cr:LiSAF laser far off the gain peak: tunable sub-200-fs pulses near 1 μm,” *Appl. Opt. Vol. 60, Issue 29*, pp. 9054–9061 **60**(29), 9054–9061 (2021).
52. J.F. Pinto, L. Esterowitz, G.H. Rosenblatt, Frequency tripling of a Q-switched Cr:LiSAF laser to the UV region. *IEEE J. Sel. Top. Quantum Electron.* **1**(1), 58–61 (1995)
53. P. Pichon, F. Druon, J.-P. Blanchot, F. Balembois, P. Georges, LED-pumped passively Q-switched Cr:LiSAF laser. *Opt. Lett.* **43**(18), 4489 (2018)
54. U. Demirbas, “Off-surface optic axis birefringent filters for smooth tuning of broadband lasers,” *Appl. Opt.* **56**(28), (2017).
55. A. Isemann, P. Wessels, C. Fallnich, Directly diode-pumped Colquiriite regenerative amplifiers. *Opt. Commun.* **260**(1), 211–222 (2006)
56. B. Sumpf, P. Adamiec, M. Zorn, H. Wenzel, G. Erbert, Nearly Diffraction Limited Tapered Lasers at 675 nm with 1 W Output Power and conversion efficiencies above 30%. *IEEE Photonics Technol. Lett.* **22**(99), 266–268 (2011)

Publisher's Note Springer Nature remains neutral with regard to jurisdictional claims in published maps and institutional affiliations.